Macromolecular Bioscience
www.mbs-journal.de

3D Bioprinted Hydroxyapatite or Graphene Oxide Containing Nanocellulose-Based Scaffolds for Bone Regeneration

Markel Lafuente-Merchan, Sandra Ruiz-Alonso, Fátima García-Villén, Alaitz Zabala, Ana M. Ochoa de Retana, Idoia Gallego, Laura Saenz-del-Burgo, and Jose Luis Pedraz**

Bone tissue is usually damaged after big traumas, tumors, and increasing aging-related diseases such as osteoporosis and osteoarthritis. Current treatments are based on implanting grafts, which are shown to have several inconveniences. In this regard, tissue engineering through the 3D bioprinting technique has arisen to manufacture structures that would be a feasible therapeutic option for bone regenerative medicine. In this study, nanocellulose–alginate (NC–Alg)-based bioink is improved by adding two different inorganic components such as hydroxyapatite (HAP) and graphene oxide (GO). First, ink rheological properties and biocompatibility are evaluated as well as the influence of the sterilization process on them. Then, scaffolds are characterized. Finally, biological studies of embedded murine D1 mesenchymal stem cells engineered to secrete erythropoietin are performed. Results show that the addition of both HAP and GO prevents NC–Alg ink from viscosity lost in the sterilization process. However, GO is reduced due to short cycle autoclave sterilization, making it incompatible with this ink. In addition, HAP and GO have different influences on scaffold architecture and surface as well as in swelling capacity. Scaffolds mechanics, as well as cell viability and functionality, are promoted by both elements addition. Additionally, GO demonstrates an enhanced bone differentiation capacity.

1. Introduction

Bone is a connective tissue which is part of the skeletal system. Its main function is to provide mobility and protection to organs. In addition, it is involved in blood cell generation and homeostasis maintenance as well as in mineral storage and blood pH regulation.[1] It is characterized by having high porosity, vascularity, and strong mechanical properties.[2–4]

Due to its characteristics, bone tissue has the potential to regenerate by itself in case of minor injuries. However, this capacity is limited and becomes ineffective in case of excessive damage such as in big traumas, bone infections, and tumors.[1,5] Furthermore, bone degenerative diseases that are closely related to the increase in population age are becoming more prevalent. Among them, osteoporosis and rheumatic diseases such as osteoarthritis have gained notoriety.[1,5]

Current therapeutic treatment is based on prosthesis implantation. Among the implant materials, metals such as titanium, ceramics, and polymers such as polyethylene have been commonly used. However, they still present some drawbacks in terms of high rigidity,

M. Lafuente-Merchan, S. Ruiz-Alonso, F. García-Villén, I. Gallego, L. Saenz-del-Burgo, J. L. Pedraz
NanoBioCel Group
Laboratory of Pharmaceutics
School of Pharmacy
University of the Basque Country (UPV/EHU).
Paseo de la Universidad 7, Vitoria-Gasteiz 01006, Spain
E-mail: laura.saenzdelburgo@ehu.eus; joseluis.pedraz@ehu.eus

The ORCID identification number(s) for the author(s) of this article can be found under https://doi.org/10.1002/mabi.202200236

DOI: 10.1002/mabi.202200236

M. Lafuente-Merchan, S. Ruiz-Alonso, F. García-Villén, I. Gallego, L. Saenz-del-Burgo, J. L. Pedraz
Biomedical Research Networking Center in Bioengineering Biomaterials and Nanomedicine (CIBER-BBN). Health Institute Carlos III.
Paseo de la Universidad 7, Vitoria-Gasteiz 01006, Spain

M. Lafuente-Merchan, S. Ruiz-Alonso, F. García-Villén, I. Gallego, L. Saenz-del-Burgo, J. L. Pedraz
Bioaraba
NanoBioCel Resarch Group
Vitoria-Gasteiz 01009, Spain

A. Zabala
Mechanical and Industrial Manufacturing Department
Mondragon Unibertsitatea
Loramendi 4, Mondragón 20500, Spain

A. M. O. de Retana
Department of Organic Chemistry I
Faculty of Pharmacy and Lascaray Research Center
University of the Basque Country (UPV/EHU)
Paseo de la Universidad 7, Vitoria 01006, Spain

lack of integration in native tissue and the absence of biodegradability and bioactivity properties.[6,7] On the other hand, bone transplantations have arisen as an alternative treatment to overcome the aforementioned problems. Nevertheless, autografts and allografts are related to the risk of donor site morbidity, chronic pain, and graft supply limitations. Moreover, in xenografts transplantations, the risk of pathogen transmission should be added.[8] In addition, it is common for patients who have undergone bone surgery to present long recovery times, high rates of implant rejection, and the necessity to have recurrent surgeries.

In this context, in order to avoid the aforementioned drawbacks, 3D bioprinting has gained notoriety when it comes to fabricating implantable structures for bone substitutes or regeneration. As an additive technique, 3D bioprinting has the advantage of creating scaffolds in a fast, automatic, and reproducible manner.[9] The technique is based on the layer-by-layer deposition of a bioink, which may be composed of a wide range of biomaterials and cell types.[9,10] In addition, bioactive molecules such as drugs, growth factors, and genetic material can be included.[10] In this regard, to manufacture scaffolds for bone regeneration, the bioink and, therefore, the bioprinted scaffold must meet certain requirements such as being biodegradable, bioactive, and biocompatible.[11]

Hydroxyapatite (HAP) is an inorganic ceramic formed of calcium and phosphate $Ca_{10}(PO_4)_6(OH)_2$.[12] As native bone is composed of 70% of HAP, it has been widely used as a biomaterial to create structures for bone regeneration.[12,13] In fact, it has been shown to be bioactive and osteoconductive as well as to provide excellent mechanical properties.[14] Moreover, due to its high porosity, HAP scaffolds have been reported to promote cell migration and osteogenic differentiation.[14,15] It has also been proven that HAP improves cell attachment and integration to native tissue in metallic implants that have been previously covered with this ceramic.[12]

Lately, graphene has gained a presence in different fields such as optics, engineering and electronics due to its excellent electroconductivity, and thermochemical and mechanical properties. Graphene oxide (GO) is formed by a sheet of sp2 hybridized carbon atom with oxygen containing functionalities.[16] This chemical derivative has been widely applied in biomedicine as a drug, protein, genes, and peptide carrier for its controlled delivery. In the tissue engineering field, GO-based hydrogels have been shown to be biodegradable, biocompatible, and enhance the mechanical rigidity of manufactured structures.[16,17] Consequently, GO has been used for the regeneration of tissues that require high mechanical strength such as bone or vascular tissue.[17] In addition, it has been reported that GO promotes osteogenesis in metal implants as well as mineralization. Furthermore, proliferation and osteogenic differentiation of mesenchymal stem cells (MSCs) have been observed after GO addition in vitro and in vivo.[8,18]

In summary, both HAP and GO have been shown to have interesting properties to be used in the formulation of bioinks for bone regeneration. However, for bioprinting, not only must these bioactive properties be taken into account, but also other important bioink characteristics such as printability and crosslinking procedure.[11] For good printability, bioinks should have adequate rheological properties. Thus, it is necessary to add a rheological modifier such as nanofibrillated cellulose (NC). In addition, NC has shown to have good mechanical properties and cytocompatibility.[19] On the other hand, sodium alginate (Alg) has been proposed due to its instant gel formation with divalent cations such as calcium.[20] Alg is a well-known polysaccharide in the tissue engineering field as it is biocompatible, biodegradable, and nontoxic.[20,21] In fact, Alg and NC have been already applied to manufacture scaffolds through 3D bioprinting for bone regeneration.[19,22]

In this study, NC–Alg–HAP and NC–Alg–GO bioinks were developed for the manufacturing of scaffolds through 3D bioprinting for bone regeneration. First, ink rheological properties and biocompatibility were evaluated. Afterward, the sterilization process was analyzed. Then, scaffolds were printed to analyze the printability, swelling, and degradation kinetics. Finally, D1 MSCs modified to produce erythropoietin hormone (D1-MSCs-EPO) were included in the NC–Alg–HAP and NC–Alg–GO inks in order to observe cell proliferation, viability, and functionality. Additionally, cell osteogenic differentiation was assayed to evaluate the application of NC–Alg–HAP and NC–Alg–GO scaffolds for bone regeneration purposes.

2. Experimental Section

2.1. Materials

Hydroxyapatite was purchased from Merck (Madrid, Spain). Graphene oxide was obtained from Graphenea (San Sebastian, Spain). Ultrapure low-viscosity high guluronic acid sodium alginate (UPLVG) was acquired from FMC Biopolymer (Sandvika, Norway). Nanofibrillated cellulose was purchased from Sappi Europe (Brussels, Belgium). Fetal calf serum (FCS), fetal bovine serum (FBS), and penicillin/streptomycin (P/S) were acquired from Gibco (San Diego, CA, USA). 3-(4,5-dimethylthiazol-2-yl)-2,5-diphenyltetrazoliumbromid (MTT) in vitro toxicology assay, calcium chloride, D-mannitol, dexamethasone, β-glycerophosphate, L- ascorbic acid, alginate lyase, and sodium citrate were obtained from Merck, (Madrid, Spain). LIVE/DEAD Viability/Cytotoxicity kit was obtained from Life Technologies (Madrid, Spain). Alamar blue was acquired from Bio-Rad científica (Madrid, Spain). Dulbecco's phosphate-buffered saline (DPBS) code BE17-513F was obtained from Lonza (Porriño, Spain). Murine D1-MSCs were obtained from ATCC (Virginia, USA).

2.2. Inks Development

Two inks were proposed. In order to formulate NC–Alg–HAP ink, HAP was dispersed at 1% (w/v) in a 2% (w/v) Alg solution. Then, NC was added at 80% (v/v) of the final solution and everything was mixed to obtain a homogeneous ink. Likewise, NC–Alg–GO ink was prepared by dispersing a GO solution of 50 μg mL^{-1} in a 2% (w/v) Alg solution. Afterward, NC was included at 80% (v/v) of the final solution and everything was homogenized to obtain the ink.

2.3. Inks Characterization

2.3.1. Rheological Study

Inks' rheological properties were analyzed by performing two different assays; steady flow measurement and oscillatory shear measurement. In the first study, viscosity was evaluated by conducting a shear rate sweep from 0.1 to 100 s^{-1} followed by a subsequent shear rate from 100 to 0.1 $s^{-1.}$ Meanwhile, the viscoelasticity properties in terms of elastic modulus (G') and viscous modulus (G'') were obtained in the oscillatory shear measurement establishing 2% of strain and an oscillation frequency sweep from 0.1 to 100 Hz. In addition, Tan δ values were acquired from the G''/G' relation. All the measurements were conducted on an AR100 rheometer from TA Instruments (New Castle, USA) with a flat 40 mm stainless steel plate and at room temperature.

2.3.2. Cytotoxicity Analysis

In vitro cytotoxicity of NC–Alg–HAP and NC–Alg–GO inks was evaluated through three different assays; adhesion, direct and indirect assays. In order to perform all the studies, circular structures were printed and mouse L929 fibroblasts from ATCC (Virginia, USA) at 3.123×10^4 cells cm^{-2} cell density were used. Cells were culture in EMEM supplemented with 10% (v/v) FCS and 1% (v/v) P/S at 37 °C in humidified 5% CO_2 atmosphere. In the adhesion test, cells were seeded onto the printed disks and cell viability was measured after 4 h of incubation. As controls, cells directly seeded onto a culture plate were used. Conversely, in the direct and indirect tests, cells were seeded onto culture plates and were maintained in DMEM for 24 h. Then, printed disks were placed onto seeded cells in the direct assay and, DMEM which had been in touch with the NC–Alg–HAP or NC–Alg–GO printed disks, were added in the indirect contact assay. After 24 of incubation, cell viability was measured in both tests. Cells with no disk exposure were used as controls. To determine cell viability in all the assays, MTT in vitro toxicity assay kit was used following the manufacturer's recommendations, and the absorbances were obtained at 570 nm with a reference wavelength of 650 nm using an Infinitive M200 microplate reader from TECAN Trading AG (Männedorf, Switzerland). Six independent samples were conducted.

Each experiment was carried out following the ISO 10993-5-2009 rule.[23] Cell viability was calculated applying Equation (1) and a cell viability above 70% was considered as nontoxic

$$\text{Cell viability } (\%) = \frac{\text{Testing sample OD570}}{\text{Untreated blank OD570}} \times 100 \quad (1)$$

2.3.3. Inks Sterilization Test

The sterilization process of NC–Alg–HAP and NC–Alg–GO inks was carried out in a short cycle autoclave by AJL Ophthalmic (Miñano, Spain) in accordance with a previous study.[24] An industrial autoclave F0A2/B model was used with a maximum of 123–124 °C temperature and 3.60–3.70 bar pressure. The sterilization was performed in 3.04 min.

Then, the repercussions of the sterilization process on inks properties were analyzed. First, inks physical appearance was observed. Then, rheological measurements were conducted as previously described (see Section 2.3.1).

2.3.4. Fourier Transform Infrared (FT-IR) Analysis of Graphene Ink

FT-IR spectra were performed with a Nicolet is 10 spectrometer from Thermo Scientific (Madrid, Spain) using an attenuated total reflectance technique. The spectra were obtained in the range 4000–500 cm^{-1} at room temperature, with a resolution of 4 cm^{-1} and 32 scans.

2.4. 3D Printing

Scaffolds were printed by using an extrusion-based 3D bioprinter Bio X from Cellink (Gothenburg, Sweden). The scaffolds' shape consisted of a circular grid-like form of 15 mm diameter and two layers. Different printing parameters were set depending on the ink. To print NC–Alg–HAP ink, a 22 G conical needle was used and printing parameters were established at 15–18 kPa printing pressure and 4–5 mm s^{-1} printing speed. On the other hand, NC–Alg–GO ink was printed using a 27 G conical needle, 22–25 kPa printing pressure, and 4–5 mm s^{-1} printing speed. NC–Alg ink was printed as control ink using the same parameters to NC–Alg–GO ink. Subsequently, all printed scaffolds were crosslinked by submerging them in a 100 mM calcium solution for 5 min.

Afterward, macroscopic pictures were taken in a Nikon AZ100 microscope from Izasa Scientific (Barcelona, Spain) to evaluate the printability.

2.5. Scaffold Characterization

2.5.1. Surface and Architectural Characterization

Cryo-SEM images were acquired in a TM-4000 Scanning Electron Microscope from Hitachi (Illinois, USA). Scaffolds were in a hydrated state and were frozen a −20 °C using a cryogenic module. Afterward, samples were observed using a 5 kV voltage.

Hydrated NC–Alg–HAP and NC–Alg–GO scaffolds were characterized with an optical profilometer from Sensofar S-NEOX (Barcelona, Spain) in order to evaluate their surface and architecture. A focus variation method was utilized. Then, to process all the data a metrological software SensoMAP Premium 7.4 from Digital Surf (Besançon, France) was used.

Architectural characterization was acquired by measuring an area of $6484 \times 4880\ \mu m^2$ at three locations on three independently printed scaffolds. A 10× objective (side sampling: 1.29 µm, vertical resolution: 25 nm) was used for each condition.

Scaffold surface evaluation was carried out by measuring three independent areas of $873 \times 656\ \mu m^2$ on the scaffolds with a 20× objective (lateral sampling: 0.65 µm, vertical resolution: 8 nm).

2.5.2. Swelling

NC–Alg–HAP and NC–Alg–GO scaffolds were lyophilized in a Telstar cryodos Freeze Dryer (Terrassa, Spain) in order to evaluate their swelling behavior. Freeze-drying process was performed

in 40 h. First, samples were progressively frozen at −50 °C for 3 h. Then, primary drying process was carried out in which chamber pressure and temperature were set at 0.2 mbar and −50 °C, respectively. After 5 h, the pressure was maintained but the temperature increased at 20 °C for 7 h. Finally, chamber pressure was removed and secondary drying process was conducted at a 20 °C during 24 h. After that, their dried weight was obtained. Then, samples were submerged in DPBS with calcium and magnesium at 37 °C to determine their swelling capacity. Finally, at selected time points, scaffolds were removed from DPBS, water excess was eliminated using filter paper and they were reweighted. NC–Alg constructs were utilized as control. The assay was carried out in triplicate and, at every time point, the swelling % was calculated applying Equation (2)

$$\text{Swelling } (\%) = \frac{W_{\text{wet}} - W_{\text{dried}}}{W_{\text{dried}}} \times 100 \quad (2)$$

where W_{wet} corresponds to wet weight and W_{dried} is dried weight.

2.5.3. Degradation Study

Degradation study of NC–Alg–HAP and NC–Alg–GO scaffolds was performed by measuring their area. Then, printed constructs were submerged in DMEM at 37 °C. Afterward, at chosen time points, scaffolds were removed from DMEM to measure their area again. Subsequently, constructs were returned to the DMEM. The study was conducted in triplicate and NC–Alg constructs were used as control. The area loss in % was calculated by applying Equation (3)

$$\text{Area loss } (\%) = \frac{A_{\text{before}} - A_{\text{after}}}{A_{\text{before}}} \times 100 \quad (3)$$

where A_{before} and A_{after} correspond to scaffold area before placing them in DMEM and after passing chosen time in the culture media, respectively.

2.5.4. Mechanical Properties Evaluation

Mechanical properties of printed scaffolds were carried out in a TA.XT.plusC Texture Analyser from Aname Instrumentación Cientifica (Madrid, Spain). A cylinder probe of 5 kg and 20 mm was used to perform all the experiments. Measurements were conducted in a compression test form by setting a 0.5 mm s^{-1} test speed and a maximum of 80% strain. Compression Young's modulus was calculated from the slope of the stress/strain curve. Six replicates per scaffold were performed and NC–Alg scaffolds were applied as controls.

2.6. Cell Culture and 3D Bioprinting

To perform the 3D bioprinting procedure, first, NC–Alg–HAP and NC–Alg–GO inks were prepared as aforementioned (see Section 2.2). Then, bioinks were prepared by mixing the inks with murine D1-MSCs engineered to secrete erythropoietin hormone (D1-MSCs-EPO) at 5×10^6 cell mL^{-1}.[25]

Cell culture was carried out in T-flasks with DMEM supplemented with 10% (v/v) FBS and 1% (v/v) P/S. Cells were cultured in a humidified atmosphere containing 5% CO_2 and at 37 °C. Culture medium was frequently substituted and at 80% of confluence, they were subcultured.

Finally, scaffolds were manufactured through the 3D bioprinting technique as previously mentioned (see Section 2.4). Afterward, they were placed in a complete medium for their culture. NC–Alg bioink was prepared and bioprinted as control. The whole procedure was carried out under aseptic conditions and at room temperature.

2.7. In Vitro Biological Evaluation

2.7.1. Cell Viability Assay by Fluorescence Microscopy

Cell viability was qualitatively evaluated with the LIVE/DEAD Viability/Cytotoxicity Kit. First, scaffolds were washed with DPBS and incubated in a staining solution containing 100 mM calcein AM for 40 min protected from the light and at room temperature. Then, the calcein solution was removed and a 0.8 μM ethidium homodimer-1 was added. After an incubation of 10 min at 37 °C, constructs were rinsed in DPBS and observed in a Nikon TMS microscope (Virginia, USA) with an excitation/emission wavelength of 495/515 nm for the calcein AM staining and 495/635 nm for the ethidium homodimer staining. Three independent assays were evaluated for each condition and the ImageJ software was used to analyze the acquired pictures in order to quantify the percentage of live and dead cells.

2.7.2. Metabolic Activity Study

D1-MSCs-EPO metabolic activity was determined by using the Alamar Blue assay (AB). The assay was carried out by depositing bioprinted scaffolds in a solution containing 10% AB in a complete medium. Then, samples were incubated at 37 °C for 4 h. Finally, fluorescence was determined in an Infinitive M200 microplate reader from TECAN Trading AG (Männedorf, Switzerland). It was set at an excitation wavelength of 560 nm and an emission wavelength of 590 nm. Scaffolds with no embedded cells were used as negative controls. At least, six samples were conducted for each condition.

2.7.3. EPO Secretion Quantification

EPO secretion was assayed using Quantikine IVD Human EPO ELISA Kit from R&D Systems (Madrid, Spain). At days 1, 7, 14, and 21 after bioprinting, scaffolds were placed with 500 μL of DMEM at 37 °C for 24 h. Then, supernatants were examined to quantify EPO secretion. Supernatants from scaffolds without cells were used as negative controls. Three independent samples for each condition were conducted.

2.8. Osteogenic Differentiation

D1-MSCs into NC–Alg, NC–Alg–HAP, and NC–Alg–GO scaffolds were differentiated to osteoblasts. Bioprinted constructs

were cultured in an osteogenic differentiation medium composed of complete culture media supplemented with 100 nM dexamethasone, 20 mM β-glycerophosphate, and 50 μM L-ascorbic acid. They were cultured for 21 days and the differentiation medium was replaced every 3 days. A complete medium without supplements was utilized to culture the controls.

2.8.1. Mineralization Assay

Mineralization evaluation of cells inside bioprinted scaffolds was carried out with Alizarin Red S staining, purchased from Merck (Madrid, Spain). At 21 days after bioprinting, scaffolds were removed from the differentiation culture medium and were washed with PBS. Next, they were fixed with 4% formaldehyde for 30 min. Afterward, Alizarin Red S solution was added to stain calcium deposits. Finally, scaffolds were washed and were observed under a Nikon AZ100 microscope.

2.8.2. Alkaline Phosphatase (ALP) Activity Quantification

ALP activity was determined after maintaining the bioprinted scaffolds in the osteoinductive medium for 1 and 21 days. First, scaffolds were disaggregated by incubating them in 1 mg mL^{-1} alginate lyase solution at 37 °C for 15 min. Next, ALP activity was quantified by using Alkaline Phosphatase Assay Kit (fluorometric). The assay was performed following the manufacturer's recommendations and fluorescence was read at 360 and 440 nm excitation/emission wavelength, respectively. Three replicates were conducted per condition.

2.8.3. RT-PCR

The osteogenic effect of NC–Alg–HAP, NC–ALG–GO, and NC–Alg scaffolds was determined using a quantitative real-time PCR study. First, a solution of 1.5% (w/v) sodium citrate and 1 mg mL^{-1} alginate lyase were applied to disaggregate the scaffolds. Then, TRIzol reagent, from Merck (Madrid, Spain), was added to extract the total mRNA. Afterward, the total mRNA was measured with a SimpliNano nanodrop from GE Healthcare Life Sciences (Madrid, Spain) and was converted to cDNA applying the Fast Gene Scriptase II, cDNA Synthesis Kit from Genetics Nippon Europe (Düren, Germany). Finally, real-time PCRs were conducted with StepOnePlus Real-Time PCR Systems from Fisher Scientific (Madrid, Spain). The specific primers for *RUNX2, ALP, osteocalcin (OSTC), and osteopontin (SPP1)* were used to determine the target genes by using a fluorogenic qRT-PCR-based (TaqMAN) assay. Glyceraldehyde-3-phosphate dehydrogenase (GAPDH) was used as the housekeeping gene. Gene expression was normalized to GAPDH and to gene expression of undifferentiated samples. The $2^{-\Delta\Delta CT}$ method was applied to calculate the relative expression of all the genes.

2.9. Statistics

Statistical analysis was conducted with IBM SPSS software. Data were indicated as mean ± standard deviation. Significant differences were considered when $p < 0.05$. To determine significant differences between two groups student's *t*-test was used, whereas ANOVA was applied to analyze multiple groups. Depending on the results of the Lavene test of homogeneity of variances, Tamhane post hoc test or Bonferroni test was utilized. Mann-Whitney nonparametric test was used to analyze non-normally distributed data.

3. Results and Discussion

Natural polymers have been shown to be excellent components to develop ink for 3D bioprinting since they are biocompatible and biodegradable. Thus, we previously fabricated a bioink composed of NC and Alg, which showed good printability and suitability with cells.[24] In this research work, we have focused on the improvement of NC–Alg bioink in order to regenerate bone tissue. For this purpose, two different inorganic components were added. HAP which apart from being the main element in the bone extracellular matrix, has been reported to be biocompatible, osteoinductive, and reinforce the bone mechanics.[12,26] We have previously demonstrated that by reinforcing gelatin scaffolds with this type of HAP, good osteoinductive properties together with excellent biocompatibility in vitro and in vivo were obtained.[27] HAP concentrations above 3% resulted in printing needle obstruction in a previous screening process. Therefore, ceramic concentration in the NC–Alg ink was reduced to 1%, which has been probed to promote cell viability and bone differentiation ability on Alg scaffolds.[28] On the other hand, GO was added since it has been gained notoriety in biomedicine. As a consequence of its ability to bond with diverse biomolecules such as DNA, proteins, and antibodies, it has been used as drug delivery system, protein carrier or biosensor component.[29,30] In tissue engineering fields, it has been reported to favour osteogenic differentiation of cells and to supply the hydrogels with excellent mechanical properties.[17] In a previous study, it was concluded that the 50 μg mL^{-1} of GO was the best concentration for cell viability and functionality in Alg microcapsules.[31] In fact, it was reported that GO concentrations above 50 μg mL^{-1} may induce cellular damage and toxicity.[30] In this regard, the effect of adding these two elements on inks properties as well as on scaffolds characteristics was evaluated. Additionally, their influence on cell viability, functionality and osteogenic differentiation was assayed.

3.1. Rheological Study

NC–Alg ink was modified by adding separately HAP and GO. Then, rheological behavior was evaluated in **Figure 1**. In steady flow measurement (Figure 1A), all the studied inks showed similar results, which consisted of shear-thinning flow behavior followed by a thixotropic behavior. Shear-thinning behavior is a characteristic of pseudoplastic materials and suggested the suitability of the inks with extrusion-based bioprinting since ink viscosity must be decreased to go through the printing needle. In addition, thixotropy indicated a viscosity recovery after being the ink extruded, which ensured the shape of the printed structure. Although all inks types showed this behavior and were suitable for extrusion bioprinting, no differences were observed when HAP or GO were included to the NC–Alg ink. It was reported in another research work that either HAP or GO may increase the viscosity values of the inks.[18,32] However, these inorganic materials

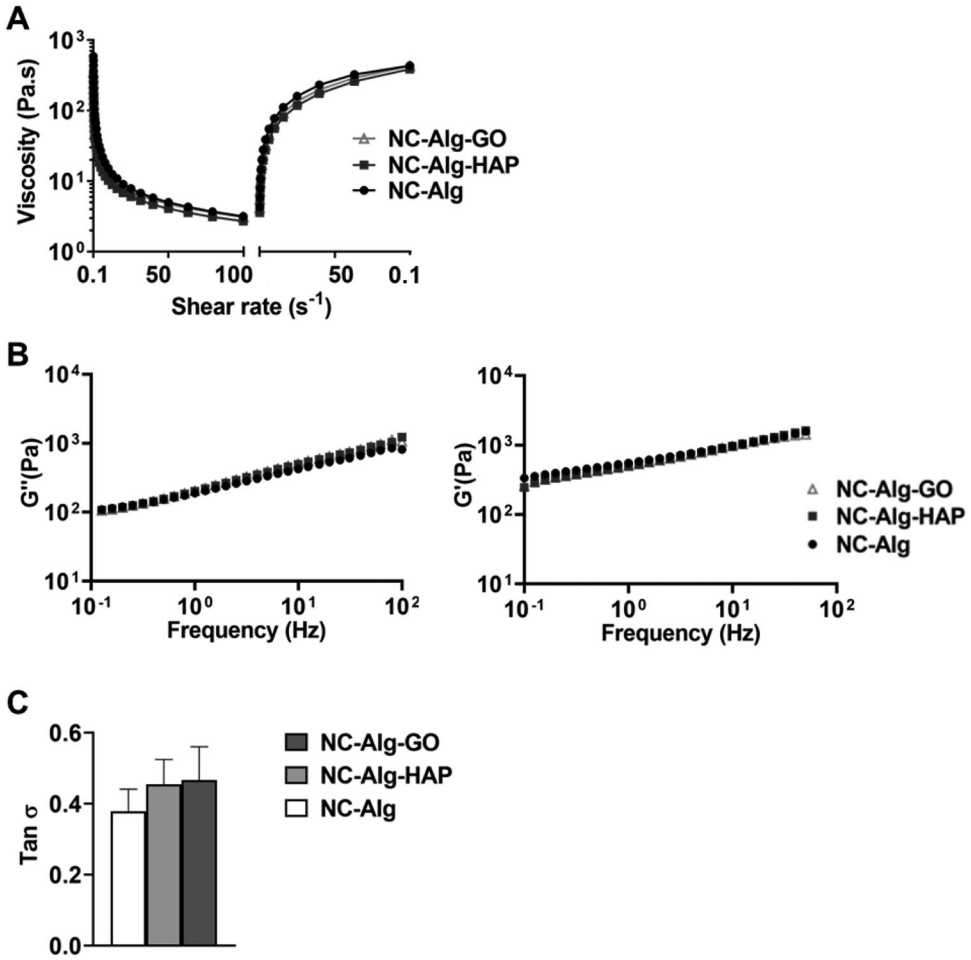

Figure 1. Rheological characterization of NC–Alg, NC–Alg–HAP, and NC–Alg–GO inks. A) Steady flow measurement. B) Viscoelasticity measurement in terms of G' and G'' moduli. C) Relationship between G''/G' expressed in tan δ. Values represent mean ± SD.

are not considered rheological modifiers. Therefore, the viscosity of the inks increased with the concentration of HAP and GO inside the inks, which were higher than the concentrations used in our study. On the other hand, in Figure 1B, viscoelasticity behavior was analyzed in terms of elastic modulus G' and viscous modulus G''. All the inks demonstrated a more elastic behavior than a viscous performance. Moreover, the addition of HAP or GO resulted in no changes in viscoelasticity values in comparison with the NC–Alg ink. Then, the G'/G'' relation was calculated with the Tan δ value in Figure 1C. Results showed no statistical differences among the inks, being all of them between 0.3 and 0.5. According to the literature, inks with Tan δ closer to 1 showed more fluidity and, therefore, scaffold shape fidelity is difficult to obtain: by contrast, with values closer to 0, inks showed more robust behavior, which compromised extrusion. In addition, viscoelasticity and Tan δ are related to cell viability within the inks. Thus, very fluid inks do not have the necessary viscosity to protect the cells from the forces exerted in the bioprinting process, while very robust inks require high printing pressures that damage the cell viability. In this study, all the inks showed a Tan δ value that is optimal for maintaining high cell viability, good shape fidelity, and uniform extrusion.[33]

3.2. Sterilization Effects Evaluation

3D printing differs from 3D bioprinting in the inclusion into the ink of the biological component, which is usually composed of cells. However, this step requires an absence of pathogens or microorganisms that may damage the cells. Consequently, developed inks were sterilized in a short cycle autoclave and, after that, they were characterized again by rheology to verify whether the sterilization process has any effect on their composition. In a previous study, the short cycle autoclave showed to be the best option to sterilize NC–Alg inks, despite the fact that it was demonstrated to cause a slight decrease in terms of viscosity and viscoelasticity values (**Figure 2**C) in comparison with nonsterilized NC–Alg inks.[24] In this study, however, as Figure 2AI,BI shows, the addition of HAP or GO, resulted in no differences in viscosity values between nonsterilized and sterilized inks. Indeed, both inks maintained shear-thinning and thixotropic behavior, which suggested excellent printability and scaffold fabrication. Similarly, NC–Alg–HAP and NC–Alg–GO inks were not affected by short autoclave when viscoelasticity values of sterilized and nonsterilized inks were compared (Figure 2BI,II).

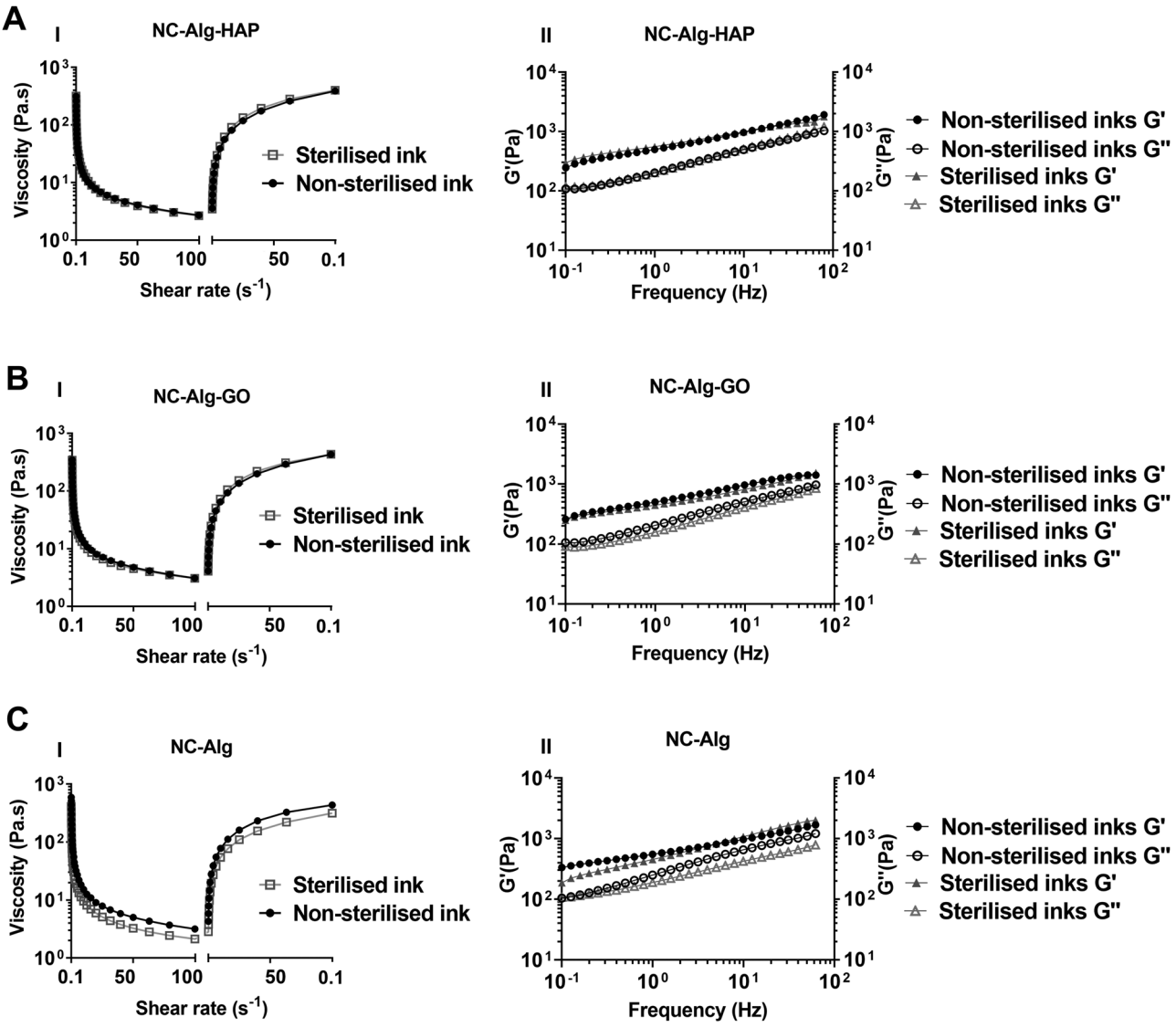

Figure 2. Rheological evaluation of inks after autoclave sterilization. A) NC–Alg–HAP ink, B) NC–Alg–GO ink, and C) NC–Alg ink. (I) Steady flow measurement. (II) Viscoelasticity measurement.

The rheological properties of HAP composites depend on suspension concentration and pore size. It has been reported that HAP is stable at temperatures below 500 °C,[34] therefore, it was expected to maintain its chemical composition and, as a consequence, had no influence on ink rheological properties. Importantly, HAP addition prevented NC–Alg ink from a rheological properties' reduction. It was previously shown that HAP prevented Alg-based hydrogel from temperature decomposition. According to this study, HAP may have displaced sodium ions of alginate avoiding its degradation. Consequently, Alg–HAP hydrogels showed higher mass after high temperature exposition which could be related to rheological properties maintenance after sterilization.[35]

On the other hand, the GO containing ink showed similar behavior to NC–Alg–HAP in terms of no rheological alteration. GO has been reported to reinforce polymeric inks in terms of stiffness and strength.[36] Thus, NC–Alg–GO ink could have higher mechanical properties than NC–Alg ink and, therefore, demonstrates greater resistance to the sterilization process.

According to rheological measurements, both sterilized inks demonstrated good properties to be printable through extrusion bioprinting. However, sterilized NC–Alg–GO ink showed a color change, becoming darker than nonsterilized ink (data not shown). Consequently, an additional study was carried out with this ink in order to verify any chemical modification as a consequence of the sterilization process. To do so, FT-IR analysis was conducted (**Figure 3**). Results showed differences between short cycle autoclaved NC–Alg–GO ink and the nonsterilized one. These spectra differences were predominantly found between carbon and oxygen bonds. A peak was detected at 1763 cm^{-1} wave number in nonsterilized ink corresponding to C=O stretching vibration. Additionally, in nonsterilized ink peaks were detected at 1204 and 1077 cm^{-1} wave numbers related to C–O and C–O–C stretching vibrations, respectively. Finally, a C–OH stitching

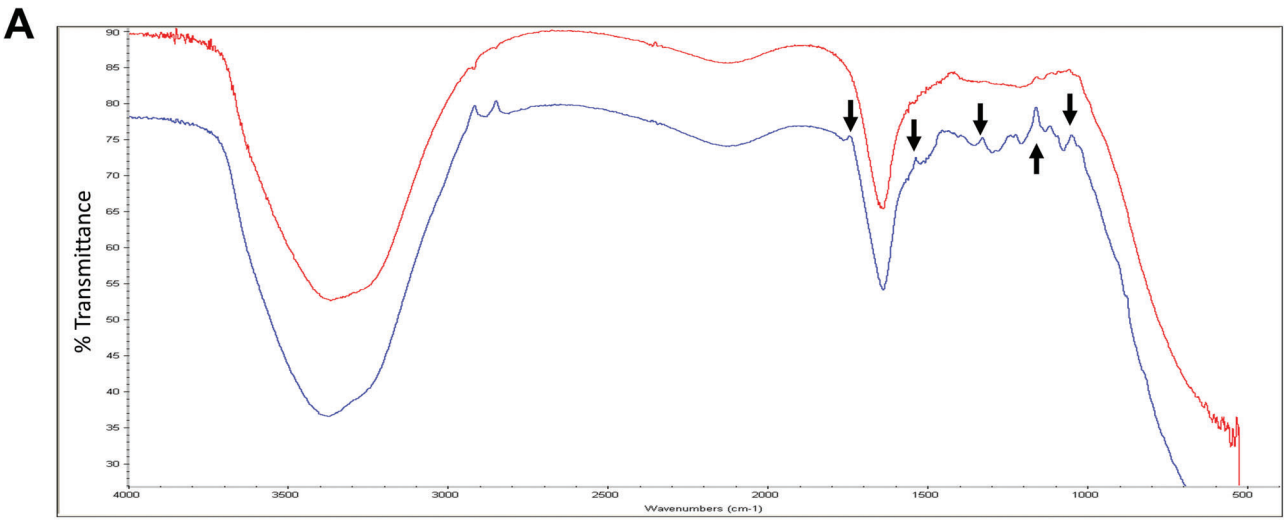

B

Sample	C=O cm^{-1}	C-O cm^{-1}	C-OH cm^{-1}	C-O-C cm^{-1}
Non-sterilised NC-Alg-GO	1763	1204	1299 1131	1077
Sterilised NC-Alg-GO	-	-	-	-

Figure 3. FT-IR assay of NC–Alg–GO ink before and after short cycle autoclave sterilization. A) FT-IR spectra showing the % transmittance differences. In red: sterilized ink; in blue: nonsterilized ink. B) Table of the signaled results from FT-IR spectra.

vibration was measured on 1299 and 1131 cm^{-1} wave numbers in nonsterilized ink. By contrast, in the sterilized NC–Alg–GO ink all these peaks were not detected, indicating bonds loss between carbon and oxygen molecules. Therefore, it can be concluded that GO was reduced due to the autoclave process. The lack of oxygen containing functional groups in reduced GO has been correlated with an increase in cell toxicity in comparison with GO.[37] Likewise, thermally reduced GO has been related to cell death and genotoxicity.[38] Consequently, the short cycle autoclave technique was discarded to sterilize NC–Alg–GO inks. As an alternative, the NC–Alg ink was sterilized by autoclave and GO was subsequently included after being sterilized with UV.

3.3. Cytotoxicity Study

Cytotoxicity study of sterilized NC–Alg–HAP and NC–Alg–GO inks was conducted to analyze their biocompatibility (**Figure 4**). In the direct contact assay, results showed high L929 fibroblasts viability when both, HAP and GO were added to NC–Alg ink. In addition, in the indirect contact assay, cell viability was also high for all the ink types. Taking into account that in both assays the cell viability was above 70%, it can be concluded that the inks have good biocompatibility. By contrast, in the adhesion assay, statistically ($p < 0.01$) lower cell viability was observed in GO containing inks in comparison with NC–Alg inks. It has been reported that

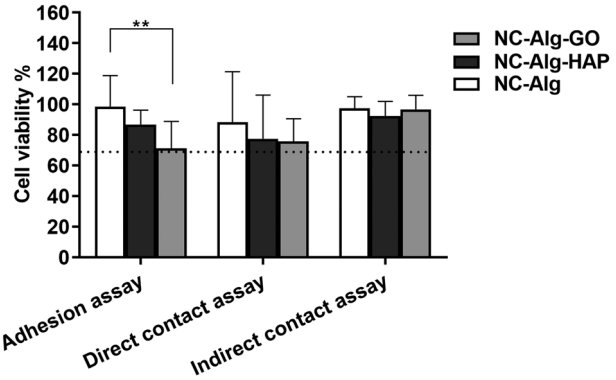

Figure 4. Cytotoxicity study of NC–Alg–HAP and NC–Alg–GO inks by adhesion, direct contact, and indirect contact assays. NC–Alg ink was used as control. Values represent mean ± SD. ** $p < 0.01$.

GO has adhesive properties.[39] In fact, previous work showed good adherence of L929 fibroblasts to a GO monolayer.[40] However, they used a longer cell incubation time before cell viability measurement than in the study, which could explain the observed low cell viability. In any case, cell viability was higher than 70%, which would indicate good biocompatibility.

The properties that GO has cells to be adhered, have been previously reported.[39] In fact, a research work demonstrated the

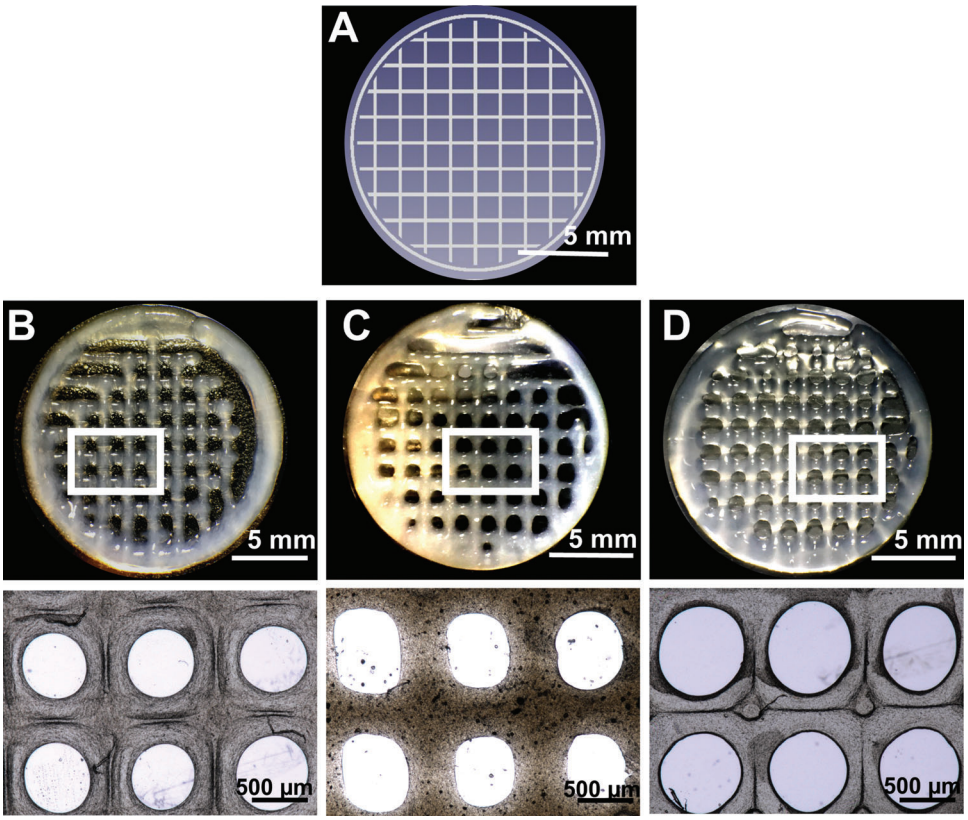

Figure 5. Printability assay. Macroscopic pictures of printed scaffolds. A) Computerized design of the scaffolds. B) NC–Alg, C) NC–Alg–HAP, and D) NC–Alg–GO. Scale bar: 5 mm and 500 µm.

good adherence of L929 fibroblasts to a GO monolayer.[40] Therefore, the low cell viability showed on NC–Alg–GO inks could be because the incubation time was shorter than in the rest of the consulted research works. In any case, cell viability was higher than 70%, which would indicate good biocompatibility.

3.4. Printability Evaluation

15 mm diameter grid-like scaffolds were printed through extrusion 3D bioprinting technique. A 27 G conical needle was used and printing parameters of 22–25 kPa pressure and 4–5 mm s^{-1} speed were set since printable scaffolds with good shape fidelity were manufactured with NC–Alg inks in previous studies.[24,41] In addition, no differences among the inks were observed in rheological measurements, therefore, it was expected to have the same printability properties. However, printing difficulties in terms of needle obstruction were observed with NC–Alg–HAP inks. Consequently, HAP containing scaffolds were printed using a higher diameter needle of 22 G, and, to maintain a constant extrusion flow, printing pressure was reduced to 15–18 kPa. By contrast, NC–Alg–GO scaffolds were properly printed by setting the same printing parameters and needle diameter as NC–Alg scaffolds. These printing differences were due to the HAP particles that blocked the narrowest needle. In fact, HAP particle size was around 200–300 µm, while GO average flake size was from nm up to 10 µm. After printing, scaffold general and in-depth images were acquired (**Figure 5**). Results showed an acceptable printability with NC–Alg–HAP and NC–Alg–GO inks compared to the computerized design (Figure 5A). Furthermore, a slight improvement could be observed in the scaffolds that contained inorganic components compared to the control, probably due to the enhancement in mechanical properties of these materials,[17,42] thus, making them more stable than NC–Alg inks. Upon closer examination, no differences were observed among the scaffolds. All of them presented an oblong grid structure with a similar grid area measurement (NC–Alg–HAP 0.41 ± 0.05 mm^2, NC–Alg–GO 0.38 ± 0.10 mm^2, and NC–Alg 0.42 ± 0.03 mm^2).

3.5. Scaffold Structure Characterization

The architecture and surface of printed NC–Alg–HAP and NC–Alg–GO scaffolds were characterized using SEM and optical profilometer techniques. As shown in **Figure 6** scaffolds structure was different depending on the addition of HAP and GO. In fact, the scaffolds containing HAP presented a flatter architecture in the SEM images compared to those containing GO, which showed more concavity (Figure 6A). These results were confirmed by optical profilometry pictures where the HAP scaffolds showed a height of around 200–300 µm at intersections, while those containing GO showed a greater height (400–500 µm). When a comparison was made with the NC–Alg scaffolds, it was shown that the differences in the scaffold architecture were due

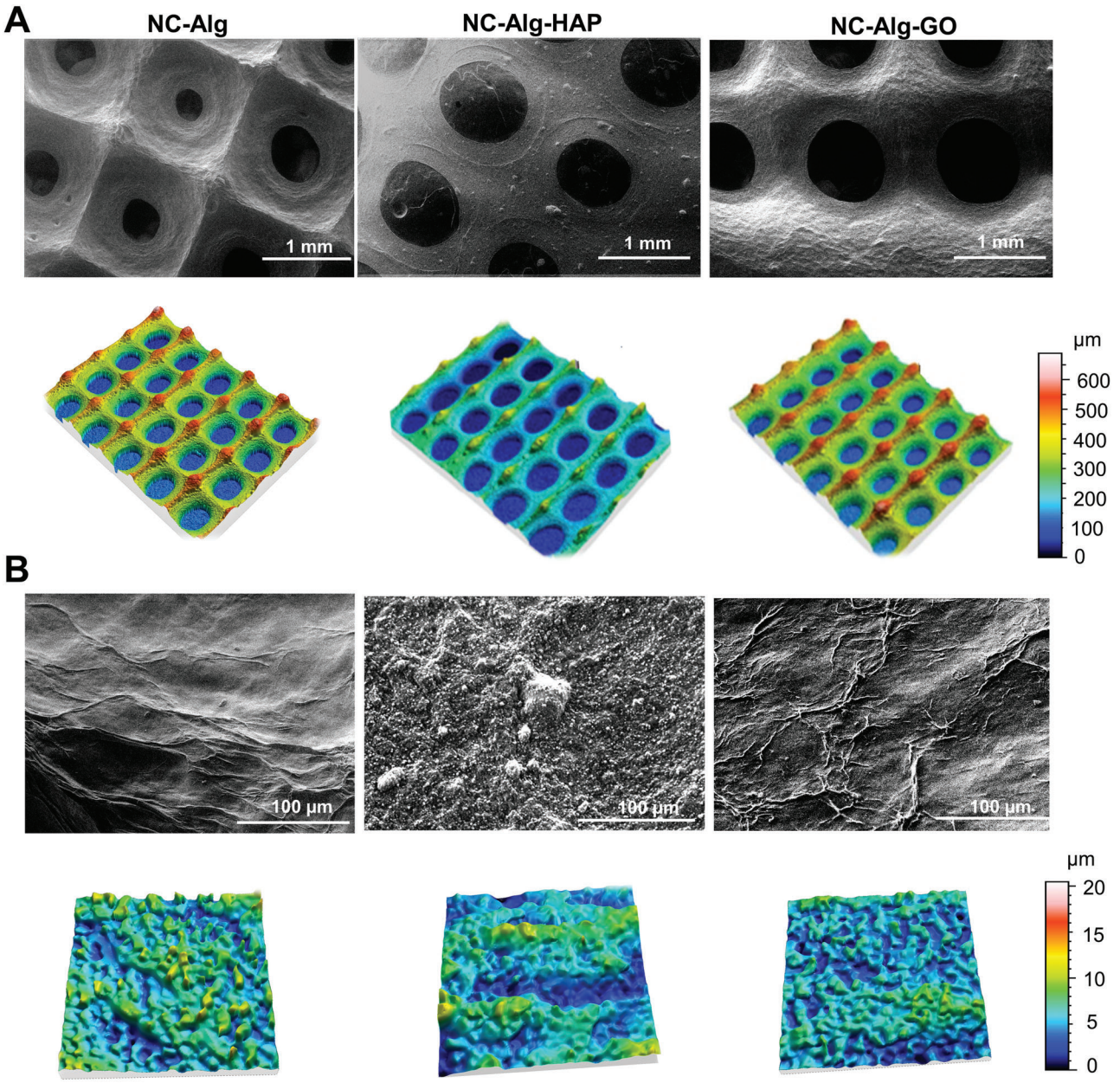

Figure 6. Printed scaffold characterization. Representative SEM images of NC–Alg, NC–Alg–HAP, and NC–Alg–GO scaffolds. Optical profilometer images of the scaffolds 3D topographical measurements. A) Architecture characterization. B) Surface evaluation. Scale bar: 1 mm and 100 μm.

to the HAP, since the GO scaffolds showed a similar architecture to the controls. The characterization was carried out after the crosslinking procedure with $CaCl_2$ aqueous solution. Therefore, it could be theorized that the hydrophilicity of the polymers together with the properties of GO to capture water molecules,[43] made both, NC–Alg–GO and NC–Alg scaffolds, more swollen than the NC–Alg–HAP scaffolds. On the contrary, HAP particles inside the scaffold matrix could cause hydrophilicity lost, and thus, achieving to flatten the scaffolds. These results were verified later in the swelling study.

On the other hand, the surface of the scaffolds was characterized in order to evaluate their roughness. Scaffolds roughness is an important parameter since it has been described that scaffolds with rougher surfaces tend to enhance MSCs adhesion and osteogenic differentiation in comparison with smooth scaffolds.[44] Furthermore, rough implants have been demonstrated to be more successful than smoothest ones.[45] Consequently, several studies covered different implant types such as titanium ones to enhance successful implantation in vivo as well as in the clinics. According to optical profilometer images in Figure 6B, all the scaffolds showed a similar surface roughness between 0 and 10 μm. However, when SEM pictures were observed, different surface roughness was shown. In fact, the HAP containing scaffolds demonstrated a granulose surface due to HAP particles. By

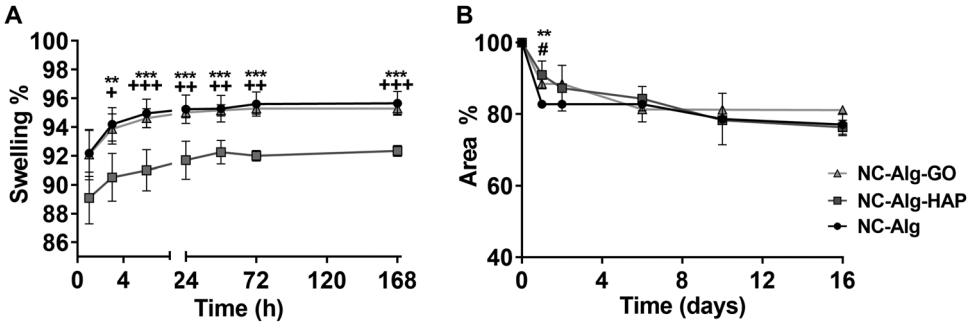

Figure 7. Characterization of NC–Alg–HAP, NC–Alg–GO, and NC–Alg scaffolds. A) Swelling assay. B) Degradation study. Values represent mean ± SD. *** $p < 0.001$; ** $p < 0.01$ comparison between NC–Alg–HAP and NC–Alg. +++ $p < 0.001$; ++ $p < 0.01$; + $p < 0.05$ comparison between NC–Alg–HAP and NC–Alg–GO. # $p < 0.05$ comparison between NC–Alg–GO and NC–Alg scaffolds.

contrast, GO scaffolds had a fibrous surface appearance that was similar to NC–Alg scaffolds. This fibrous roughness could be due to NC fibers in the scaffold. These results were in concordance with other research works in which the addition of HAP to the scaffolds proved to increase their roughness and, therefore, cell viability and osteogenic differentiation.[46] Regarding the GO, another work reported similar results in terms of no roughness increase after GO addition in titanium scaffolds.[47] Nevertheless, all the scaffolds showed a rough surface, which would indicate good cell adhesion, the promotion of cell osteogenic differentiation and excellent implantability in bone tissue.

3.6. Swelling and Degradation Study

A swelling (S) study was carried out in order to analyze the water uptake capacity of all the printed constructs. Swelling capacity is related to scaffold permeability and, therefore, to the transport of nutrients and gases into the scaffold.[48] In this study, as **Figure 7**A shows, in all the scaffolds the percentage of swelling increased until the equilibrium was reached within 24 h. In addition, all the scaffolds showed high water uptake capacity, which suggests good permeability and cell nourishment. It has been previously described that inks composed of Alg or NC have high water uptake capacity due to the hydrophilic characteristics of the polymers.[49] Importantly, differences among scaffolds were observed when inorganic components such as HAP and GO were added. S% was statistically lower in NC–Alg–HAP scaffolds in comparison with NC–Alg–GO and control scaffolds in the majority of time points. It was expected that by adding HAP the water uptake capacity would be reduced since HAP particles did not leave space for water particles. It has also been reported that the swelling capacity decreased while HAP concentrations increased in scaffolds.[42] By contrast, NC–Alg–GO scaffolds demonstrated the same swelling properties as NC–Alg scaffolds, which indicated that the inclusion of GO particles did not displace water molecules. In fact, it has been widely described the capacity of graphene molecules to create strong hydrogen bonds with water molecules[43] and, therefore, the GO-containing scaffolds swelling properties are high. These swelling properties have been also showed in another study in which increasing GO concentrations resulted in higher water absorption.[50] Despite the fact of swelling reduction due to HAP, all scaffolds showed high swelling properties (>90%), which suggested excellent nutrient transport into the scaffold.

For regenerative medicine applications, scaffold degradation kinetics should be taken into account to determine its applicability. When it comes to bone, the implanted scaffolds must be stable with a controlled degradation rate to enable bone regeneration. In this regard, a degradation assay of NC–Alg–HAP and NC–Alg–GO scaffolds was performed for 16 days (Figure 7B). Both scaffolds showed similar degradation kinetics being the main area loss in the first days of the assay. Importantly, scaffolds containing HAP or GO demonstrated less area loss in comparison with NC–Alg scaffolds at the beginning of the study. In fact, this resistance to the degradation process was statistically significant in HAP scaffolds ($p < 0.01$) and in GO scaffolds ($p < 0.05$) within 24 h of the assay. At the end of the assay, all the scaffolds showed a similar area loss that was around 20%. The degradation study indicated a controlled degradation behavior of NC–Alg–HAP and NC–Alg–GO scaffolds, suggesting good stability of the scaffolds, which is essential for the early stages of bone regeneration.[51] Furthermore, the degradation kinetics may be modified depending on medical applications. It has been reported that varying molecular weight of the alginate as well as by chemical modifications such as phosphorylation could accelerate or reduce scaffold degradation kinetics.[52] Likewise, the degradation rate could be influenced by reducing the particles size and increasing the porosity of the HAP or by the chemical modification of the GO.[17,53]

3.7. Mechanical Properties Evaluation

Mechanics in bone are fundamental for proper tissue functionality such as movement support and organ protection.[3] Consequently, scaffolds and grafts to be implanted require adequate mechanical properties. For this reason, compression Young's modulus was acquired since it is a material parameter that represents the material's resistance or stiffness to deformation under load. As it is shown in **Figure 8**, Young's modulus parameter increased significantly ($p < 0.001$) when HAP and GO were added to the NC–Alg ink. Interestingly, GO containing scaffolds demonstrated higher mechanical properties than HAP scaffolds ($p < 0.001$). It has been widely described that both inorganic elements enhanced scaffold mechanical properties.[14,17] HAP has been

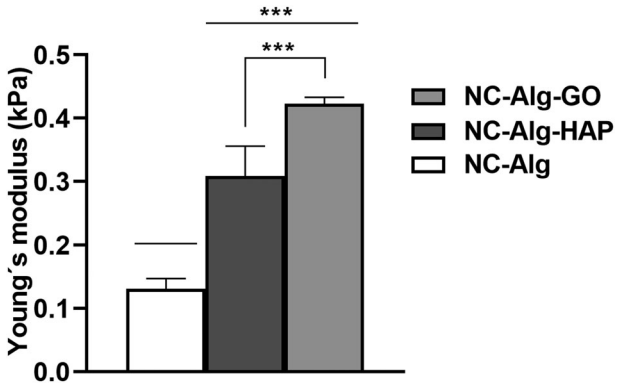

Figure 8. Young's modulus measurements of printed NC–Alg–HAP, NC–Alg–GO, and NC–Alg scaffolds. Values represent mean ± SD. *** $p < 0.001$.

used to fabricate orthopedic implants since it has been demonstrated to be a mechanically competent material with similar physical properties to native bone tissue. In addition, by increasing HAP concentrations, scaffold mechanical properties may be improved as it has been proven in gelatin-based hydrogels.[42] Similarly, GO has been reported to have superior mechanical properties. As a result, it has been applied to reinforce materials for diverse purposes such as electronics and mechanics.[16] In the tissue engineering field, GO has been utilized to improve scaffolds' mechanical properties because of the reinforcing effect of GO in the polymer matrix.[54] Despite the fact that both materials increased scaffold mechanical properties, were far from bone mechanical properties (10–20 GPa).[55] Bone is a stiff tissue and it is difficult to obtain similar mechanics with scaffolds based on soft hydrogels. According to the literature, similar mechanics to those of bone could be obtained by using metals such as titanium, bioglasses or synthetic polymers such as polycaprolactone.[56] In this regard, either ceramic scaffold based only on HAP or high GO concentration composites have shown to be mechanically similar to bone, therefore, increasing HAP and GO concentrations on the ink would improve mechanical properties. However, biocompatibility and printability would be compromised.

Taking into account these results, NC–Alg–HAP and NC–Alg–GO scaffolds could be used in local injuries to support the regeneration of damaged bone or to partial bone ruptures.

3.8. Cell Viability and Functionality Study

Good cell survival and functionality inside the scaffold will ensure clinical applicability for bone regeneration purposes. For this reason, D1-MSCs-EPO were added to the NC–Alg–HAP and NC–Alg–GO inks, and their biological response in terms of cell metabolism, viability and EPO release was evaluated within 21 days of bioprinting. Cell density was established at 5×10^6 cells mL^{-1} in order to avoid problems when evaluating cells in vitro, since cells death due to extrusion pressures of the bioprinter together with low cell densities within the bioink proved to be unsatisfactory for obtaining clear results in a previous study.[24] Cell metabolic activity was measured weekly for 21 days (**Figure 9**A). Results showed that the metabolism of cells embedded in all the scaffolds increased over time. Importantly, scaffolds containing HAP and GO demonstrated higher cell metabolic activity along the study compared to NC–Alg scaffolds. Furthermore, the improvement in cell metabolic activity was significant in NC–Alg–HAP scaffolds on days 1, 7 ($p < 0.001$) and 14 ($p < 0.05$) after bioprinting in comparison with control scaffolds. Likewise, cells embedded in GO containing scaffolds showed a significantly higher ($p < 0.001$) metabolic activity at the first time points of the assay when it was compared to NC–Alg scaffolds. These results suggested cell proliferation within the scaffolds after bioprinting. Furthermore, the addition of HAP and GO into the NC–Alg based bioink improved the metabolic activity of embedded cells, suggesting that cells were more viable and functional than those inside control bioinks. These results were in concordance with other studies in which the HAP inside polymeric scaffolds enhanced cell migration and viability.[12] Similarly, it has been reported that the metabolic activity of stem cells was higher in the presence of GO.[57] On the other hand, HAP and GO containing sterile bioinks showed an improvement in the rheological properties that, together with the increase in the mechanical properties, suggested greater protection of the cells against the damage caused by the bioprinting process.

D1-MSCs-EPO viability was evaluated by Live/Dead assay in Figure 9B. Obtained images showed no visual differences among the scaffolds at day 1 after bioprinting. Cells inside the scaffolds were mostly alive (in green) and were well distributed throughout the scaffolds. By contrast, at day 21 after bioprinting, differences were observed between cells inside NC–Alg–HAP and NC–Alg–GO scaffolds. In fact, cells in HAP containing scaffolds tended to form aggregates while in GO scaffolds cell aggregates were not found. Cell aggregates were also visualized in the NC–Alg scaffolds. It has been reported in the literature that cell aggregates promoted osteogenic differentiation of MSCs.[58] The absence of cell aggregation inside NC–Alg–GO scaffolds could be explained with the increase in scaffold mechanics, which make the GO containing bioink stiffer than the others. Additionally, oxide derivatives of graphene have found to reduce aggregation due to its high hydrophilic nature.[59] Importantly, higher green fluorescent intensity was obtained in scaffolds containing HAP and GO in comparison with NC–Alg scaffolds, indicating higher cell viability inside scaffolds containing inorganic components. In addition, it was expected to be higher cell viability in HAP and GO scaffolds in accordance with cell metabolic activity results.

Finally, D1-MSCs-EPO were used to determine cell functionality inside bioprinted scaffolds. The quantification of this hormone was selected as it has been previously probed that it can be easily measured from cells encapsulated in Alg hydrogels.[60] As shown in Figure 9C, EPO release increased over time in all the scaffolds indicating good cell functionality after bioprinting. When a comparison was made, NC–Alg–HAP scaffolds showed higher amounts of EPO release in comparison with NC–Alg–GO and control scaffolds. Furthermore, the hormone was quantified from the first day of the assay in HAP scaffolds while in GO scaffolds EPO release was not observed until day 14 after bioprinting. Importantly, this increase in EPO release on HAP containing scaffolds was statistically significant at day 14 ($p < 0.001$). Moreover, NC–Alg scaffolds showed also a significantly higher EPO release at day 14 than NC–Alg–GO scaffolds. At the

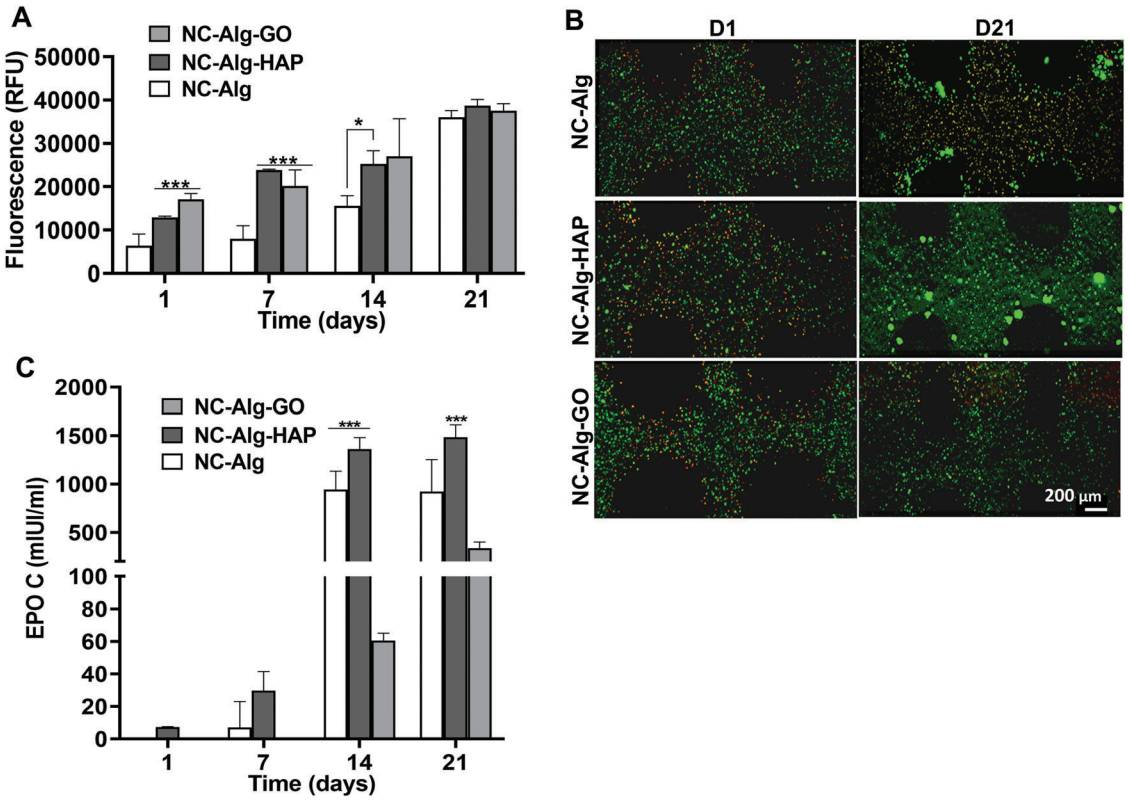

Figure 9. D1-MSCs-EPO viability and functionality assays inside NC–Alg–HAP, NC–Alg–GO, and NC–Alg scaffolds. A) Cell metabolic activity evaluation. B) Representative fluorescence pictures scaffolds at days 1 and 21 of bioprinting after live/dead staining, showing live (green) and dead (red) cells. Scale bar: 200 µm. C) EPO release assay. Values represent mean ± SD. *** $p < 0.001$; ** $p < 0.01$; * $p < 0.05$.

end of the study, NC–Alg–HAP scaffolds demonstrated higher amounts of EPO release than GO and control scaffolds ($p < 0.001$) (NC–Alg–HAP 1483.90 ± 128. 46 mLUI mL^{-1}, NC–Alg–GO 337.93 ± 63.10 mLUI mL^{-1} and NC–Alg 925.21 ± 327. 99 mLUI mL^{-1}). It can be suggested that the enhancement in EPO release in HAP scaffolds was due to the increase in its production as cell viability and cell metabolism were higher than in NC–Alg scaffolds. Furthermore, HAP has already been used as a carrier of EPO for drug delivery purposes.[61] Similar EPO production and release could be expected in cells inside GO containing scaffolds since better cell viability and metabolism were also seen than in the control scaffolds. However, GO has been described to interact with diverse molecules including proteins, therefore, it could be suspected that EPO hormone was adhered to GO, which prevented its release to the medium. This EPO adhesion has also been described in Alg–GO microcapsules.[31] In order to avoid hormone attachment to GO, the same authors proposed to cover GO with FBS or bovine serum albumin.[62] Thus, it can be assumed that EPO release may have been under quantified.

In conclusion, biological results showed that D1-MSCs-EPO cells inside HAP and GO containing scaffolds were viable, active and functional, indicating excellent biocompatibility of inorganic elements with cells. However, to determine the feasibility of these scaffolds to regenerate bone tissue, osteogenic differentiation studies were also carried out.

3.9. Osteogenic Differentiation

D1-MSCs were used to evaluate their osteogenic differentiation inside NC–Alg–HAP and NC–Alg–GO scaffolds. It has been previously described the ability of MSCs to differentiate in different cell lines such as chondrocytes, myocytes, adipocytes, and osteoblasts.[63] Therefore, they have been widely applied for tissue engineering and regenerative medicine purposes. Likewise, D1-MSCs have been used to differentiate to osteoblasts inside Alg-based hydrogels in a previous research work.[64]

First, bioprinted scaffolds were stained with Alizarin Red after being 21 days in the differentiation medium. Alizarin Red stains in red the calcium deposits, which is a characteristic of the mineralized osteogenic matrix. As shown in **Figure 10**A, all the scaffolds were stained after 21 days of culture suggesting osteogenic differentiation. On the contrary, cells inside scaffolds that were in nondifferentiated media did not produce mineralization, as the Alizarin Red staining was removed. Despite the fact that GO containing scaffolds that were treated with nondifferentiated media showed higher rests of the staining, it was concluded that this was due to the ability of GO to adhere to diverse molecules. The staining results were inconclusive in terms of evaluating whether the addition of HAP and GO had a positive effect on promoting osteogenic differentiation since NC–Alg scaffolds were also stained.

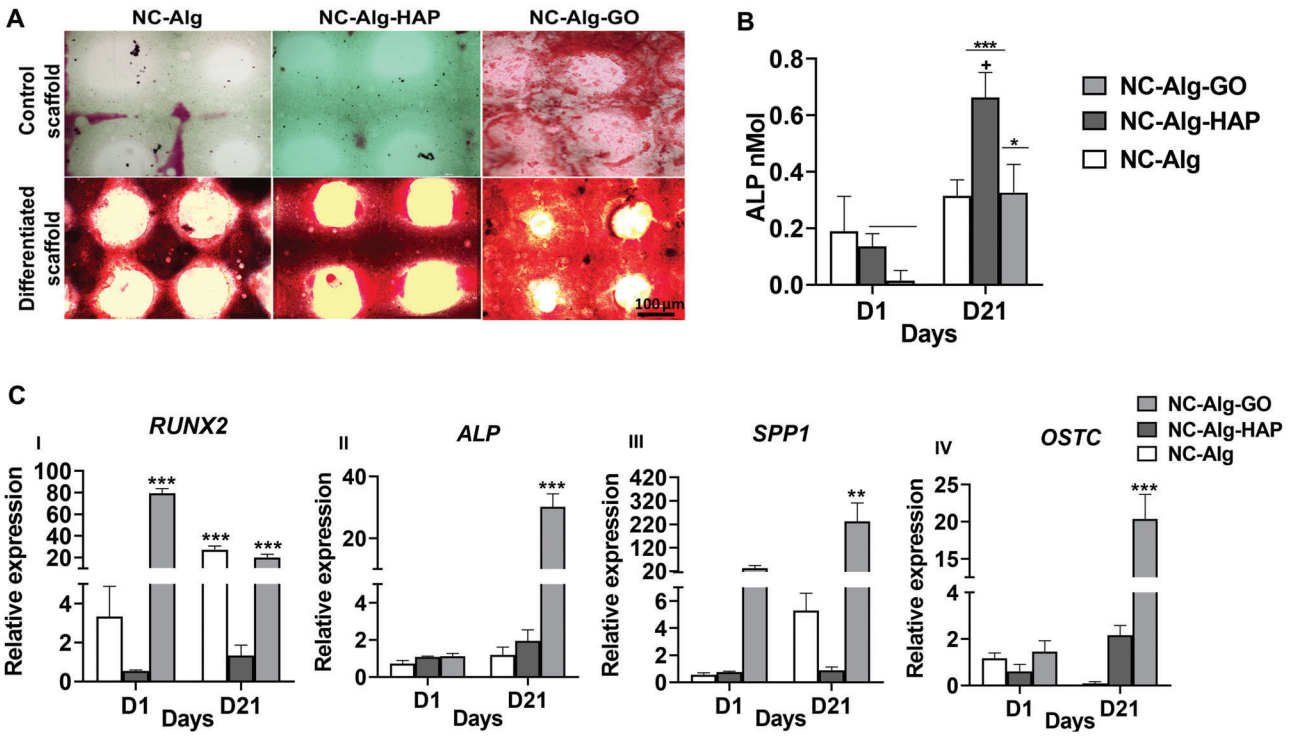

Figure 10. Osteogenic differentiation study of embedded D1-MSC. A) Alizarin red staining of NC–Alg, NC–Alg–HAP, and NC–Alg–GO scaffolds. Scale bar: 100 µm. B) Alkaline phosphatase (ALP) enzyme quantification assay at days 1 and 21 of bioprinting. C) (I–IV) Osteogenic gene expression of cells. RT-PCR was performed after 1 and 21 days. Values represent mean ± SD. *** $p < 0.001$; ** $p < 0.01$; * $p < 0.05$.

Consequently, the activity of the ALP enzyme was quantified. ALP enzyme is an osteogenic marker that is produced by osteoblasts. Therefore, the presence of ALP would indicate osteogenic differentiation. Results, showed in Figure 10B, an increase in ALP activity along the days in all the scaffolds. In addition, the enzyme activity increase was significant in HAP scaffolds ($p < 0.001$) and in GO scaffolds ($p < 0.05$). Importantly, at day 21 of the assay, cells inside NC–Alg–HAP cells demonstrated a significantly ($p < 0.05$) higher ALP production than NC–Alg–GO and NC–Alg scaffolds (0.66 ± 0.08 nmol in NC–Alg–HAP, 0.32 ± 0.10 nmol in NC–Alg–GO and 0.31 ± 0.05 nmol in NC–Alg). These results suggested the promotion of the differentiation capacity of D1-MSCs to osteoblasts due to HAP, which was previously described in the literature. It has been proved that HAP as a porous and rough material can stimulate osteogenic differentiation and osteoblast maturation.[65] As a result, the same ALP increment was observed in Alg–HAP scaffolds[28] and in NC–HAP scaffolds.[66] Regarding GO, results indicated an ALP enzyme production over time suggesting osteogenic differentiation. However, the results were similar to NC–Alg scaffolds indicating no influence on the differentiation capacity of D1-MSCs. This went against what the literature describes since osteoinductive properties have been attributed to the GO molecule. In fact, in other research works, ALP activity increased when GO was added into the bioink.[18,67] ALP upregulates early bone formation by promoting its mineralization. Low ALP levels on NC–Alg–GO ink may suggest the completion of the early calcification period and the beginning of the late maturation process of cells.[67] Furthermore, it is also known the ability of GO to adhere to diverse molecules including enzymes. Consequently, an exhaustive study on differentiation such as gene expression quantification was to perform.

Finally, RT-PCR was conducted to evaluate the relative gene expression of cells inside NC–Alg–HAP and NC–Alg–GO scaffolds. Osteogenic gene markers such as *RUNX2*, *ALP*, *OSTC*, and *SPP1* were analyzed in Figure 10C. *RUNX2* is an essential transcription factor that plays a key role in the formation of osteoblasts.[68] As shown in Figure 10CI the expression of *RUNX2* was greater ($p < 0.001$) in scaffolds containing GO at day 1 in comparison with HAP scaffolds and control. Likewise, gene expression in GO scaffolds was significantly elevated ($p < 0.001$) at day 21 when compared to HAP sample. However, it was significantly lower than in control scaffolds ($p < 0.001$). *ALP* gene is associated with osteogenic differentiation and encodes the ALP enzyme (previously analyzed in this study).[69] Results in Figure 10CII showed an increase in *ALP* expression over time in all the scaffolds. Importantly, gene expression was increased ($p < 0.001$) in GO scaffolds compared to the NC–Alg–HAP and NC–Alg scaffolds. Surprisingly, *ALP* gene expression did not agree with the results obtained from the quantification of the enzyme in which HAP scaffolds showed the greatest enzyme activity. Reviewing the literature, HAP containing hydrogels or scaffolds showed to obtain similar *ALP* gene expression and enzyme activity values to this study.[18,51,65] Likewise, other studies have demonstrated that GO promoted *ALP* gene expression which is in accordance with the results of this study.[18,67] Therefore, it can

be suggested that the quantification of ALP enzymatic activity in GO scaffolds may have been lower than it had to be. The enzyme underquantification may be due to the capacity of GO to adhere to various molecules.[70] In fact, GO has been previously used to immobilize enzymes.[71] *SPP1* gene regulates the production of osteopontin, which is a protein of the bone extracellular matrix.[72] Figure 10CIII shows that GO enhanced cells expression of the *SPP1* gene at days 1 and 21, being the gene expression at day 21 significantly higher ($p < 0.01$) than the gene expression in NC–Alg–HAP and control scaffolds. Furthermore, HAP scaffolds demonstrated less gene expression than control at the end of the assay, even though this difference was not statistically relevant. *SPP1* gene is regulated by *RUNX2* gene,[73] which could explain the low expression in HAP scaffolds. Finally, *OSTC* gene expression was assayed since it is related to mature bone.[72] Results (Figure 10CIV) showed an increase in gene expression in both, HAP and GO scaffolds over time, meanwhile gene expression was barely observed in NC–Alg scaffolds at day 21. Thus, it can be concluded bone differentiation within HAP and GO scaffolds. Interestingly, the addition of GO to the scaffold increased ($p < 0.001$) *OSTC* gene expression in comparison with HAP scaffolds.

Taking into account the differentiation study, it can be concluded that the D1-MSCs differentiated into bone cells within the NC–Alg and NC–Alg–HAP scaffolds. Furthermore, this differentiation was further promoted by adding GO to the bioink, which has been already widely described in the literature. When a comparison was made, it should be noted that osteogenic expression was considerably increased by GO, indicating greater bone differentiation of D1-MSCs than those in HAP scaffolds. This difference between HAP and GO may be occurred because of the adhesion of GO to the osteoinductive molecules such as those used in the differentiation medium.[73] Thus, making GO scaffolds more osteoinductive than HAP ones.

4. Conclusions

Inorganic components have shown to be a good option to create scaffolds for bone tissue engineering. Thus, HAP and GO have been added to NC–Alg based inks in order to evaluate whether they affect ink properties, scaffold characteristics and embedded D1-MSCs biologic behavior. No rheological differences were observed after the inclusion of HAP and GO in the ink. However, the sterilization study revealed a rheological properties maintenance after short cycle autoclave sterilization. Importantly, NC–Alg–GO ink demonstrated an incompatibility with autoclave sterilization due to a GO reduction, therefore, another sterilization method such as UV had to be carried out. Scaffold characterization study showed differences between HAP and GO scaffolds in terms of architecture and swelling properties. In fact, GO scaffolds presented higher swelling capacity and therefore, a greater height and concave structure. On the other hand, both, the addition of HAP and GO increased the scaffold stability and mechanical properties, being the GO the one that showed the greatest improvement in scaffold mechanics.

Finally, biological studies showed good biocompatibility of D1-MSC with HAP and GO since high cell metabolic activity values as well as high cell viability were observed in those scaffolds. NC–Alg–HAP scaffolds demonstrated cell differentiation to bone, but the addition of GO to the scaffolds promoted a higher expression of osteogenic markers in D1-MSC, suggesting that GO has greater osteoinductive properties than HAP. According to this study, NC–Alg–HAP and NC–Alg–GO scaffolds would be a feasible therapeutic option for bone tissue engineering, being those that contain GO the best option.

Acknowledgements

This work was financially supported by the Basque Country Government (IT907-16) and the University of the Basque Country UPV/EHU. The authors thank the Basque Government for the granted fellowship to Sandra Ruiz-Alonso (PRE_2021_2_0153). Likewise, the authors thank ICTS "NANBIOSIS", in particular by the Drug Formulation Unit (U10) of the CIBER in Bioengineering, Biomaterials and Nanomedicine (CIBER-BBN) at the University of the Basque Country (UPV/EHU) in Vitoria-Gasteiz.

Conflict of Interest

The authors declare no conflict of interest.

Data Availability Statement

Research data are not shared.

Keywords

3D bioprinting, bioinks, bone, graphene oxide, hydroxyapatite, tissue engineering

Received: June 9, 2022
Revised: July 26, 2022
Published online:

[1] P. Bhattacharjee, B. Kundu, D. Naskar, H.-W. Kim, T. K. Maiti, D. Bhattacharya, S. C. Kundu, *Acta Biomater.* **2017**, *63*, 1.
[2] G. Tozzi, A. De Mori, A. Oliveira, M. Roldo, *Materials* **2016**, *9*, 267.
[3] H. D. Kim, S. Amirthalingam, S. L. Kim, S. S. Lee, J. Rangasamy, N. S. Hwang, *Adv Healthcare Mater.* **2017**, *6*, 23.
[4] C. Wang, W. Huang, Y. Zhou, L. He, Z. He, Z. Chen, X. He, S. Tian, J. Liao, B. Lu, Y. Wei, M. Wang, *Bioact. Mater.* **2020**, *5*, 82.
[5] J. Filipowska, K. A. Tomaszewski, L. Niedźwiedzki, J. A. Walocha, T. Niedźwiedzki, *Angiogenesis* **2017**, *20*, 291.
[6] L. Roseti, V. Parisi, M. Petretta, C. Cavallo, G. Desando, I. Bartolotti, B. Grigolo, *Mater. Sci. Eng., C* **2017**, *78*, 1246.
[7] X. Bai, M. Gao, S. Syed, J. Zhuang, X. Xu, X.-Q. Zhang, *Bioact. Mater.* **2018**, *3*, 401.
[8] J. C. Boga, S. P. Miguel, D. De Melo-Diogo, A. G. Mendonça, R. O. Louro, I.-D. J. Correia, *Colloids Surf., B* **2018**, *165*, 207.
[9] W. Zhu, X. Ma, M. Gou, D. Mei, K. Zhang, S. Chen, *Curr. Opin. Biotechnol.* **2016**, *40*, 103.
[10] P. S. Gungor-Ozkerim, I. Inci, Y. S. Zhang, A. Khademhosseini, M. R. Dokmeci, *Biomater. Sci.* **2018**, *6*, 915.
[11] K. Hölzl, S. Lin, L. Tytgat, S. Van Vlierberghe, L. Gu, A. Ovsianikov, *Biofabrication* **2016**, *8*, 032002.
[12] N. Ramesh, S. C. Moratti, G. J. Dias, *J. Biomed. Mater. Res., Part B* **2018**, *106*, 2046.

[13] Q. Fu, M. N. Rahaman, F. Dogan, B. S. Bal, *J. Biomed. Mater. Res., Part B* **2008**, *86B*, 125.
[14] A. Das, D. Pamu, *Mater. Sci. Eng., C* **2019**, *101*, 539.
[15] S. T. Bendtsen, S. P. Quinnell, M. Wei, *J. Biomed. Mater. Res.* **2017**, *105*, 1457.
[16] A. Raslan, L. Saenz Del Burgo, J. Ciriza, J. L. Pedraz, *Int. J. Pharm.* **2020**, *580*, 119226.
[17] B. D. Holt, Z. M. Wright, A. M. Arnold, S. A. Sydlik, *Wiley Interdiscip. Rev.: Nanomed. Nanobiotechnol.* **2017**, *9*, 3.
[18] J. Zhang, H. Eyisoylu, X.-H. Qin, M. Rubert, R. Müller, *Acta Biomater.* **2021**, *121*, 637.
[19] M. Müller, E. Öztürk, Ø. Arlov, P. Gatenholm, M. Zenobi-Wong, *Ann. Biomed. Eng.* **2017**, *45*, 210.
[20] E. Axpe, M. L. Oyen, *Int. J. Mol. Sci.* **2016**, *17*, 1976.
[21] F. Yu, X. Han, K. Zhang, B. Dai, S. Shen, X. Gao, H. Teng, X. Wang, L. Li, H. Ju, W. Wang, J. Zhang, Q. Jiang, *J. Biomed. Mater. Res., Part A* **2018**, *106*, 2944.
[22] D. Nguyen, D. A. Hägg, A. Forsman, J. Ekholm, P. Nimkingratana, C. Brantsing, T. Kalogeropoulos, S. Zaunz, S. Concaro, M. Brittberg, A. Lindahl, P. Gatenholm, A. Enejder, S. Simonsson, *Sci. Rep.* **2017**, *7*, 658.
[23] ISO 10993-5:2009 Biological Evaluation of Medical Devices. Part 5: Tests for In Vitro Cytotoxicity. International Organization for Standardization, Geneva, Switzerland **2009**.
[24] M. Lafuente-Merchan, S. Ruiz-Alonso, A. Espona-Noguera, P. Galvez-Martin, E. López-Ruiz, J. A. Marchal, M. L. López-Donaire, A. Zabala, J. Ciriza, L. Saenz-Del-Burgo, J. L. Pedraz, *Mater. Sci. Eng., C* **2021**, *126*, 112160.
[25] H. Gurruchaga, J. Ciriza, L. Saenz Del Burgo, J. R. Rodriguez-Madoz, E. Santos, F. Prosper, R. M. Hernández, G. Orive, J. L. Pedraz, *Int. J. Pharm.* **2015**, *485*, 15.
[26] Y. Li, L. Yang, Y. Hou, Z. Zhang, M. Chen, M. Wang, J. Liu, J. Wang, Z. Zhao, C. Xie, X. Lu, *Bioact. Mater.* **2022**, *18*, 213.
[27] M. C. Echave, I. Erezuma, N. Golafshan, M. Castilho, F. B. Kadumudi, C. Pimenta-Lopes, F. Ventura, A. Pujol, J. J. Jimenez, J. A. Camara, R. Hernáez-Moya, L. Iturriaga, L. Sáenz Del Burgo, I. Iloro, M. Azkargorta, F. Elortza, R. Lakshminarayanan, T. H. Al-Tel, P. García-García, R. Reyes, A. Delgado, C. Évora, J. L. Pedraz, A. Dolatshahi-Pirouz, G. Orive, *Mater. Sci. Eng., C* **2021**, *134*, 112539.
[28] F. You, X. Chen, D. M. L. Cooper, T. Chang, B. F. Eames, *Biofabrication* **2018**, *11*, 015015.
[29] A. Raslan, J. Ciriza, A. M. Ochoa de Retana, M. L. Sanjuán, M. S. Toprak, P. Galvez-Martin, L. Saenz-Del-Burgo, J. L. Pedraz, *Pharmaceutics* **2021**, *13*, 1473.
[30] A. Raslan, L. Saenz Del Burgo, A. Espona-Noguera, A. M. Ochoa de Retana, M. L. Sanjuán, A. Cañibano-Hernández, P. Galvez-Martin, J. Ciriza, J. L. Pedraz, *Pharmaceutics* **2020**, *12*, 543.
[31] J. Ciriza, L. Saenz Del Burgo, M. Virumbrales-Muñoz, I. Ochoa, L. J. Fernandez, G. Orive, R. M. Hernandez, J. L. Pedraz, *Int. J. Pharm.* **2015**, *493*, 260.
[32] M. Maas, U. Hess, K. Rezwan, *Curr. Opin. Biotechnol.* **2014**, *19*, 585.
[33] T. Gao, G. J. Gillispie, J. S. Copus, A. K. Pr, Y.-J. Seol, A. Atala, J. J. Yoo, S. J. Lee, *Biofabrication* **2018**, *10*, 034106.
[34] K. Tõnsuaadu, K. A. Gross, L. Plūduma, M. Veiderma, *J. Therm. Anal. Calorim.* **2011**, *110*, 647.
[35] J. A. Sánchez-Fernández, G. Presbítero-Espinosa, L. Peña-Parás, E. I. R. Pizaña, K. P. V. Galván, M. Vopálenský, M. Vopálenský, I. Kumpová, L. E. Elizalde-Herrera, *Polymers* **2021**, *13*, 2927.
[36] B. G. Compton, N. S. Hmeidat, R. C. Pack, M. F. Heres, J. R. Sangoro, *JOM* **2017**, *70*, 292.
[37] J. Zhang, H.-Y. Cao, J.-Q. Wang, G.-D. Wu, L. Wang, *Front. Cell Dev. Biol.* **2021**, *9*, 616888.
[38] S. Mittal, V. Kumar, N. Dhiman, L. K. S. Chauhan, R. Pasricha, A. K. Pandey, *Sci. Rep.* **2016**, *6*, 39548.
[39] J. Ghitman, E. I. Biru, E. Cojocaru, G. G. Pircalabioru, E. Vasile, H. Iovu, *RSC Adv.* **2021**, *11*, 13653.
[40] I. Lasocka, L. Szulc-Dąbrowska, M. Skibniewski, E. Skibniewska, W. Strupinski, I. Pasternak, H. Kmieć, P. Kowalczyk, *Toxicol. In Vitro* **2018**, *48*, 276.
[41] M. Lafuente-merchan, S. Ruiz-alonso, A. Zabala, P. Gálvez-martín, J. A. Marchal, B. Vázquez-lasa, I. Garrido, L. Saenz-del-Burgo, J. L. Pedraz, *Macromol. Biosci.* **2022**, *22*, 2100435.
[42] S. Suvarnapathaki, X. Wu, D. Lantigua, M. A. Nguyen, G. Camci-unal, *Macromol. Biosci.* **2020**, *20*, 2000176.
[43] B. Lian, S. De Luca, Y. You, S. Alwarappan, M. Yoshimura, V. Sahajwalla, S. C. Smith, G. Leslie, R. K. Joshi, *Chem. Sci.* **2018**, *9*, 5106.
[44] X. Cun, L. Hosta-Rigau, *Nanomaterials* **2020**, *10*, 2070.
[45] A. Dank, I. H. A. Aartman, D. Wismeijer, A. Tahmaseb, *Int. J. Implant Dent.* **2019**, *5*, 12.
[46] W. Yang, W. Han, W. He, J. Li, J. Wang, H. Feng, Y. Qian, *Mater. Sci. Eng., C* **2016**, *60*, 45.
[47] W. Dong, L. Hou, T. Li, Z. Gong, H. Huang, G. Wang, X. Chen, X. Li, *Sci. Rep.* **2015**, *5*, 18266.
[48] H. Park, X. Guo, J. S. Temenoff, Y. Tabata, A. I. Caplan, F. K. Kasper, A. G. Mikos, *Biomacromolecules* **2009**, *10*, 541.
[49] M. Mahinroosta, Z. Jomeh Farsangi, A. Allahverdi, Z. Shakoori, *Mater. Today Chem.* **2018**, *8*, 42.
[50] J. Zhang, H. Eyisoylu, X.-H. Qin, M. Rubert, R. Müller, *Acta Biomater.* **2021**, *121*, 637.
[51] F. Xing, Z. Chi, R. Yang, D. Xu, J. Cui, Y. Huang, C. Zhou, C. Liu, *Int. J. Biol. Macromol.* **2021**, *184*, 170.
[52] E. Alsberg, H. J. Kong, Y. Hirano, M. K. Smith, A. Albeiruti, D. J. Mooney, *J. Dent. Res.*. **2003**, *82*, 903.
[53] J. G. Dellinger, A. M. Wojtowicz, R. D. Jamison, *J Biomed Mater Res A* **2006**, *77A*, 563.
[54] S. D. Purohit, R. Bhaskar, H. Singh, I. Yadav, M. K. Gupta, N. C. Mishra, *Int. J. Biol. Macromol.* **2019**, *133*, 592.
[55] C. F. Guimarã£Es, L. Gasperini, A. P. Marques, R. L. Reis, *Nat. Rev. Mater.* **2020**, *5*, 351.
[56] S. K. Nandi, A. Mahato, B. Kundu, P. Mukherjee, *Mater. Biomed. Eng.* **2019**, *2*, 21.
[57] A. Di Crescenzo, S. Zara, C. Di Nisio, V. Ettorre, A. Ventrella, B. Zavan, P. Di Profio, A. Cataldi, A. Fontana, *ACS Appl. Bio Mater.* **2019**, *2*, 1643.
[58] A. Chatterjea, V. Lapointe, A. Barradas, H. Garritsen, H. Yuan, A. Renard, C. A. Van Blitterswijk, J. De Boer, *Eur. Cells Mater.* **2017**, *33*, 121.
[59] P. Bellet, M. Gasparotto, S. Pressi, A. Fortunato, G. Scapin, M. Mba, E. Menna, F. Filippini, *Nanomaterials* **2021**, *11*, 404.
[60] A. Cañibano-Hernández, L. Saenz del Burgo, A. Espona-Noguera, G. Orive, R. M. Hernández, J. Ciriza, J. L. Pedraz, *Mol. Pharmaceutics* **2017**, *14*, 2390.
[61] K.-I. Nagasaki, T. Ikoma, S.-I. Katsuda, T. Tonegawa, J. Tanaka, T. Nakamura, H. Sato, S. Ito, N. Sasaki, T. Agui, *Vet. Med. Sci.* **2009**, *71*, 729.
[62] L. Saenz Del Burgo, J. Ciriza, A. Acarregui, H. Gurruchaga, F. J. Blanco, G. Orive, R. M. Hernández, J. L. Pedraz, *Mol. Pharmaceutics* **2017**, *14*, 885.
[63] O. Juffroy, D. Noël, A. Delanoye, O. Viltart, I. Wolowczuk, C. Verwaerde, *Differentiation* **2009**, *78*, 223.
[64] S. Nam, R. Stowers, J. Lou, Y. Xia, O. Chaudhuri, *Biomaterials* **2019**, *200*, 15.
[65] J. Fang, P. Li, X. Lu, L. Fang, X. Lü, F. Ren, *Acta Biomater.* **2019**, *88*, 503.

[66] F. Liu, B. Wei, X. Xu, B. Ma, S. Zhang, J. Duan, Y. Kong, H. Yang, Y. Sang, S. Wang, W. Tang, C. Liu, H. Liu, *Adv. Healthcare Mater.* **2020**, *10*, 2001851.
[67] Y. Jiang, D. Zhou, B. Yang, *J. Biomater. Appl.* **2022**, *37*, 527.
[68] T. Komori, *J. Cell. Biochem.* **2011**, *11*, 2750.
[69] Y. Lei, Z. Xu, Q. Ke, W. Yin, Y. Chen, C. Zhang, Y. Guo, *Mater. Sci. Eng., C* **2017**, *72*, 134.
[70] Y. Zhang, C. Wu, S. Guo, J. Zhang, *Nanotechnol. Rev.* **2013**, *2*, 27.
[71] J. Zhang, F. Zhang, H. Yang, X. Huang, H. Liu, J. Zhang, S. Guo, *Langmuir* **2010**, *26*, 6083.
[72] C. K. Huang, W. Huang, P. Zuk, R. Jarrahy, G. H. Rudkin, K. Ishida, D. T. Yamaguchi, T. A. Miller, *Plast. Reconstr. Surg.* **2008**, *121*, 411.
[73] S. H. M. Wong, S. S. Lim, T. J. Tiong, P. L. Show, H. F. M. Zaid, H.-S. Loh, *Int. J. Mol. Sci.* **2020**, *21*, 5202.